Fabrication of reduced graphene oxide decorated with CuS nanoparticles and its activity toward the adsorption of Methylene Blue

FATIMA TUZ JOHRA and WOO-GWANG JUNG*

School of Materials Science and Engineering, Kookmin University 77 Jeongneung-ro, Seongbuk-gu, Seoul 02707, Republic of Korea

Abstract: Reduced graphene oxide (RGO) can act as an adsorbent because of its high surface area. The adsorptive characteristics of a RGO composite combined with CuS were studied quantitatively. The removal efficiency of Methylene Blue was found to be about 85 %, which is higher than that of bare CuS (≈73 %). Furthermore, the kinetics of adsorption of Methylene Blue was inspected to determine the rate of the process. The removal process was faster with the RGO–CuS system than with bare CuS. Both high and low temperatures were not favorable for this adsorption process. In highly ionic media of high or low pH, the adsorption was greater than in media of neutral pH. Thermodynamic parameters were calculated in this study and they suggest that this is physisorption and exothermic in nature.

Keywords: reduced graphene oxide; copper sulfide; adsorption; kinetics; Methylene Blue.

INTRODUCTION

Graphene, a 2D hexagonal carbon structure, is a very well-known material in the scientific world because of its extraordinary electronic band structure, optical properties, and high surface area.[1,2] Chemically modified graphene obtained by reduction of graphene oxide (GO), termed reduced graphene oxide (RGO), has opened up a broad field of applications because of its ability to hold many kinds of nanoparticles. Their high surface areas make RGO-based nanoparticles more favorable for use in electrochemical applications and purification of water from hazardous materials, such as heavy metals, dyes, and oil, by photocatalysis and adsorption.[3–7]

Methylene Blue (MB) is a potent cationic dye that is widely used in the paper, cotton and wool industries. The effluents from these industries signific-

---

antly contribute to environmental pollution and hence, the decolorization of MB is important. Decolorization could be achieved by removing the MB from the solution or by degrading the MB. Adsorption is an excellent method to remove the dye from solution. Using a high surface area and low-cost adsorbent, promising results could be obtained. The development of efficient adsorbents is one of the key research subjects, especially in contaminant treatment systems. Metal sulfides are known as semiconductor according to their electronic properties. NiS, ZnS, CuS and CdS are very well known semiconductors because of their applications in energy storage, catalysts, semiconductor application and electrochemical sensors.[8–11] A few studies have been reported on the photocatalytic effect of CuS with RGO.[3,11,12] To the best of our knowledge, there are no reports on the adsorptive behavior of CuS along with RGO. Thus, a low-cost one-pot method was chosen to synthesize CuS nanoparticles in combination with RGO to investigate its adsorptive behavior towards MB. Hu *et al.* synthesized RGO–CuS nanocomposites in presence of surfactant.[13] Shi *et al*. synthesized CuS/RGO by sonochemical method in an organic solvent.[14] In most cases, an organic solvent was used to synthesize this composite.[15,16]

In the present work, the adsorptive characteristics of a CuS-decorated RGO nanocomposite in the decolorization of MB dye solutions were studied. Adsorption could be possible before photocatalysis, even during photocatalysis. Hence, the present approach was to understand the adsorption process, *i.e*., how the nanocomposite could be used to remove dyes in aqueous media. The decoration of RGO with CuS was achieved using hydrothermal treatment for a shorter time compared to previously reported works. The process is a comparatively easy and low-cost method.[17,18] After thorough characterization of the obtained product, it was used as an adsorbent for MB. The effects of pH and temperature on the adsorption isotherms and kinetics of MB adsorption by RGO–CuS were investigated.

EXPERIMENTAL

Preparation of GO

Graphene oxide (GO) was prepared by a previously reported method.[19] Three grams of powdered graphite (3 g) was mixed with 18 g of $KMnO_4$ and placed in a round-bottomed flask with a mixture of H_2SO_4 and H_3PO_4 (9:1). The mixture was heated in a mantle at 50 °C for 12 h. Thereafter, the mixture was poured into a beaker with 400 mL ice and 3 mL H_2O_2, whereby a brown solution was obtained. The solution was successively washed with deionized (DI) water, HCl and ethanol. After washing, the GO was collected by filtration and dried in an oven at 80 °C for 12 h.

Synthesis of RGO–CuS

GO suspensions were prepared by dissolving GO in DI water (0.5 mg mL^{-1}) using sonication. 0.05 M $CuCl_2$ was added to the GO suspension. After complete dissolution of the $CuCl_2$, 0.1 M thiourea was added to the solution as a precursor of sulfide to form CuS.

NH$_4$OH was used to maintain pH 9 during the reaction. This mixture was then transferred into a Teflon-lined autoclave, and the hydrothermal treatment was performed at 150 °C for 10 h. After completion of the reaction, the sample was collected by washing several times with DI water followed by filtering and drying at 60 °C for 12 h. Bare CuS nanoparticles were also synthesized in a similar way in the absence of GO.

Characterization

Morphological analysis was performed using field-emission scanning electron microscopy (FE-SEM) and energy-dispersive X-ray spectrometry (EDS) analyses using a JEOL JSM-7601 instrument. The obtained powder products were spread over pieces of carbon tape. X-Ray diffraction (XRD) analyses were performed using a Rigaku D/max 2500 (Rigaku, Japan) instrument with CuK$_\alpha$ radiation under a voltage of 40 kV and a current of 200 mA. The obtained powder product was directly analyzed in these measurements. Diffraction data were recorded for 2θ angles between 3 and 70°. Raman spectra were recorded from 500 to 3000 cm^{-1} on a Horiba Jobin Yvon LabRAM ARAMIS instrument using a 514.5 nm Ar laser at a power of 0.5 mW. The powder samples were dispersed onto a microscope slide before collection of the spectra. X-Ray photoelectron spectrometry (XPS) measurements were performed using an ESCA2000 instrument with an AlK$_\alpha$ X-ray source (1486.6 eV) at $\approx$10^{-10} Torr vacuum pressure. The pass energy was set at 50 or 20 eV for wide or narrow scanning, respectively. The X-ray take-off angle was fixed at 56°.

Adsorption technique

To investigate the adsorption abilities of RGO–CuS and bare CuS, 100 mg of adsorbent was added to a 100 mL aqueous solution of 20 ppm MB. This suspension was stirred in the dark and samples were collected at certain time intervals. The absorbance of these samples was collected at the maximum MB absorbance peak (665 nm) using a Perkin Elmer Precisely Lambda 35 UV/Vis spectrometer and the concentrations of the samples were calculated by a previously prepared calibration curve using the Beer–Lambert law. The samples were centrifuged to remove the suspended adsorbent in the solution before measurement of their absorbance. The treatment time was calculated by combining with the centrifuge time.

RESULTS AND DISCUSSION

The XRD patterns of the prepared RGO, CuS, and RGO–CuS samples are shown in Fig. 1. GO shows its characteristic peak at 10.48°, which corresponds to the (001) crystal plane. There is another peak near 43°, which corresponds to the (100) plane. The diffraction peaks in the patterns of both CuS and RGO–CuS belong to the hexagonal crystal system of CuS (JCPDS-06-0464).[20] There are no other peaks arising from GO, indicating that the RGO nanosheets did not stack during the hydrothermal process and the reduction of GO to RGO. In addition there were no other significant peak for other copper compounds (*e.g.*, CuO), which confirms the purity of the composite.

The surface morphology of the RGO–CuS was investigated by FE-SEM. Fig. 2 shows that the CuS was combined with the RGO. The EDS spectra also confirm the purity of the nanocomposite as no elements other than C, Cu, S and O were observed. The mole ratio of Cu to S was ≈1:1, as expected. The TEM and HR-TEM images are shown in Fig. 3, which reveals that the CuS nanoparticles

TUZ JOHRA and JUNG

are spread over the RGO thin sheet and that the average size of the CuS nano-
particles was 50 nm. It could be seen that the nanoparticles decorated the surface
of the RGO sheets with interplanar spacing of 0.273, 0.183 and 0.154 nm, corres-
ponding to the *d* spacing for the (103), (107) and (116) planes of hexagonal
structured CuS, respectively, which agreed with the XRD data. The synthesized
CuS in the nanocomposite is well crystalline. Thus, both the morphological and
the structural data confirm the formation of CuS along with RGO.
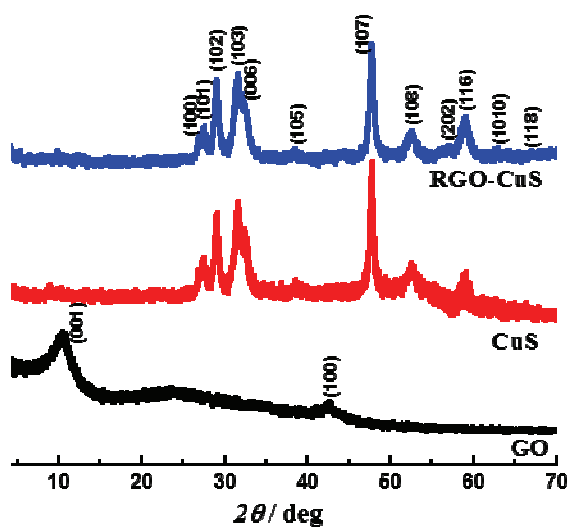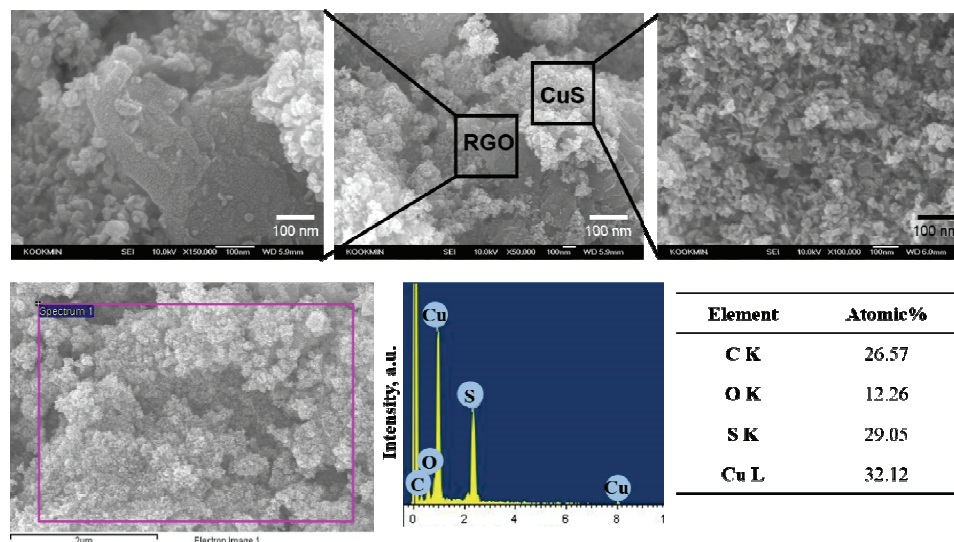

Fig. 1. The XRD patterns of GO, bare CuS and RGO–CuS.

Fig. 2. FE-SEM images and EDS spectra of RGO–CuS.

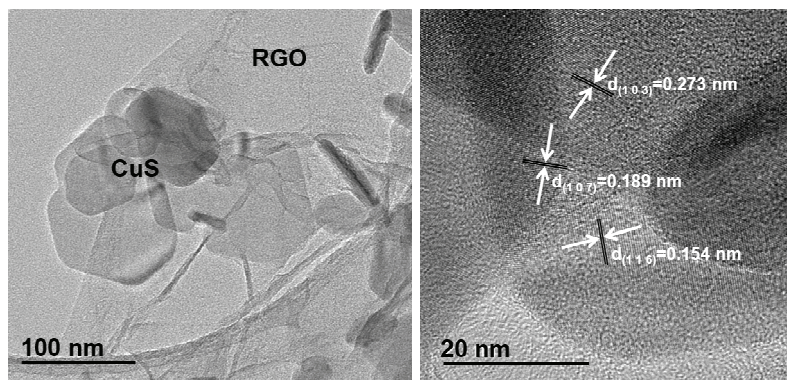| Element	Atomic%
C K	26.57
O K	12.26
S K	29.05
Cu L	32.12

Fig. 3. TEM and HR-TEM of RGO–CuS.

The reduction of GO could be confirmed from the Raman analysis. The Raman spectra of GO, bare CuS, and RGO–CuS are shown in Fig. 4. The Raman spectrum of CuS shows significant bands at 268, 474 and 924 cm^{-1}, which correspond to the A_{1g} transverse (TO), longitudinal (LO), and 2LO optical modes of the second-order Raman spectrum of CuS, respectively.[21,22] The Raman spectrum of RGO–CuS also comprises the aforementioned peaks in combination with the regular D and G peaks of the carbon component. Both the D and G peak positions are slightly shifted to lower wavenumbers for RGO–CuS compared with those for bare CuS, which indicates that graphitization occurred during reduction.[19] The D and G peaks arise from the breathing mode of κ-point phonons with A_{1g} symmetry and the E_{2g} phonon of the sp^2 C atoms, respectively.[23] The intensity ratio of the D and G peaks is inversely proportional to the average crystallite size in graphitic materials.[24] The D/G ratio for RGO–CuS (1.05) after the reduction was larger than that for GO (0.97), indicating that the average crystallite size of the sp^2 domains became smaller in RGO–CuS.
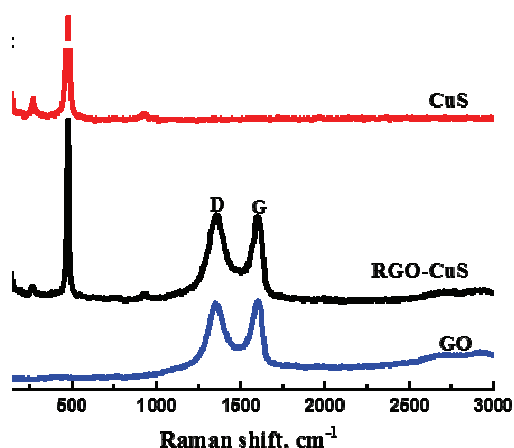

Fig. 4. Raman spectra of GO, RGO–CuS and bare CuS.

The wide-scan XPS spectra of GO and RGO–CuS, in which RGO–CuS exhibits signals due to C, Cu, S and O, are shown in Fig. 5a. The deconvoluted C 1s spectra of both GO and RGO–CuS are shown in Fig. 5b, from which it is clear that the amount of O-containing groups had decreased after the reduction of GO. The GO spectrum contains peaks at 284.6, 286.68, 288.2, and 289.11 eV, which correspond to C=C, epoxy, carbonyl and carboxyl groups, respectively[25]. After the reduction, the intensity of all bands diminished, except for the one at 284.6 eV, while the peak near 289.11 eV disappeared. The high-resolution XPS spectrum of Cu 2p shows two bands at 932.0 and 951.88 eV, which correspond to Cu $2p_{3/2}$ and Cu $2p_{1/2}$, respectively. The peak separation is about 19.88 eV, which is a typical value for the Cu^{2+} state. There are two shaken up peaks at around 945.7 and 963.7 eV, which indicate the paramagnetic chemical state of Cu^{2+}. The spectrum of S 2p in Fig. 5d shows two peaks at 162.22 and 168.58 eV corresponding to $2p_{3/2}$ and $2p_{1/2}$, respectively, with a splitting of 6.36 eV. These are consistent with the binding energy of sulfur in the sulfide state of CuS. All of these observations confirmed the formation of the RGO–CuS nanocomposite.
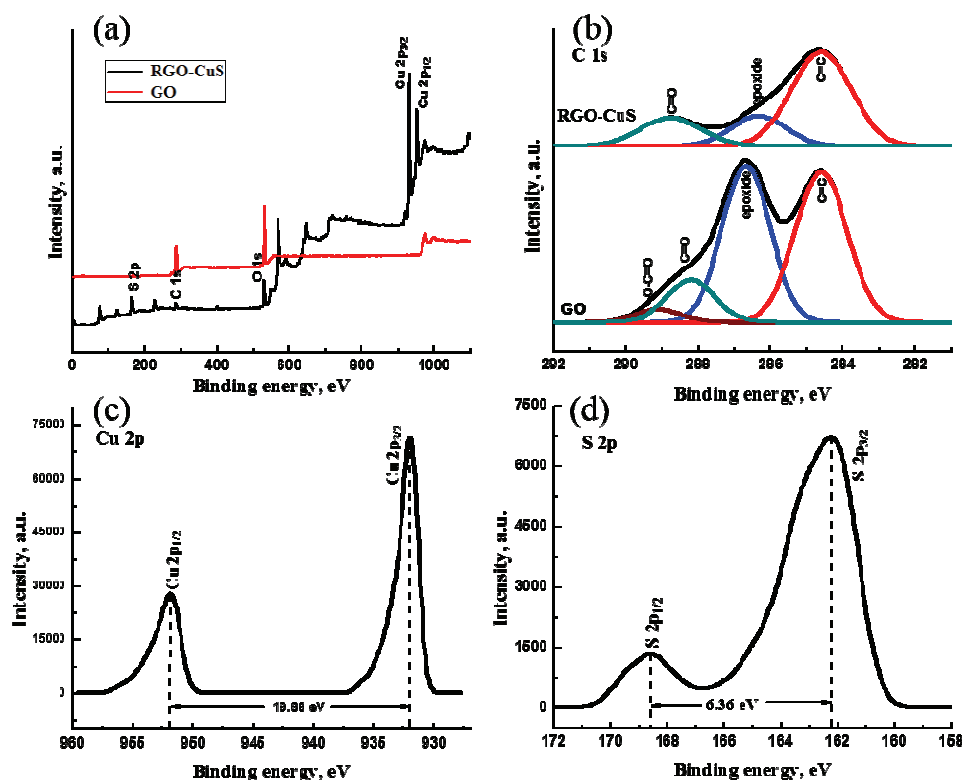

Fig. 5. XPS entire spectra (a) and C1s spectra of RGO–CuS and GO (b); Cu 2p (c) and S 2p (d) spectra of RGO–CuS.

The activity of RGO–CuS in the adsorption of MB was tested under dark conditions so that no photochemical reactions could occur. The efficiency of MB removal by RGO–CuS and that by bare CuS, for comparison, are shown in Fig. 6a.
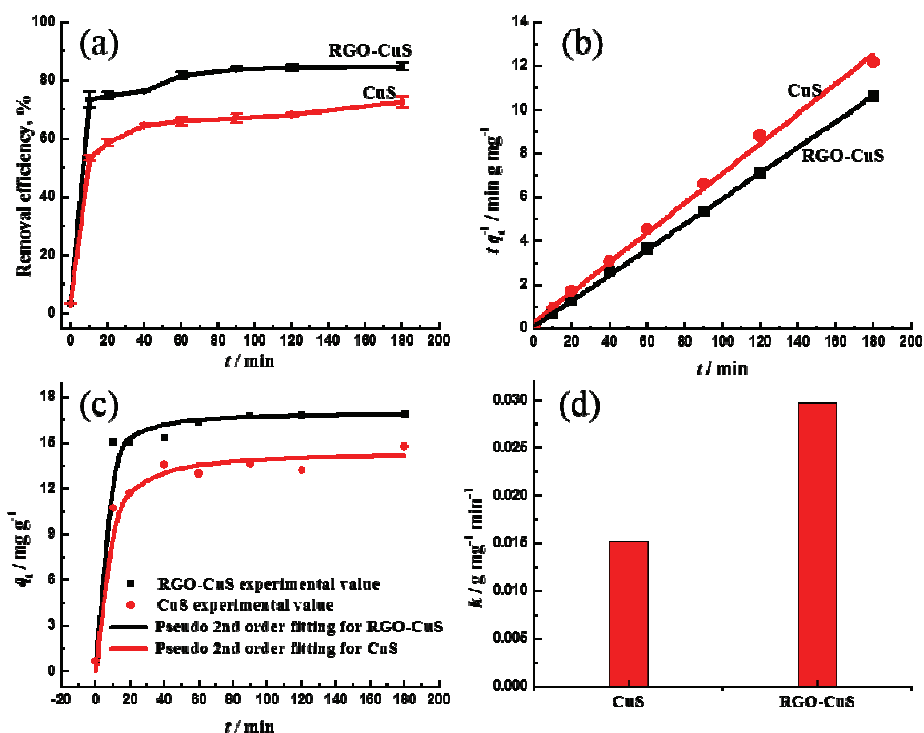

Fig. 6. a) Removal efficiency, pseudo-second order kinetic equation (b) and kinetics (c) fitting; d) comparison of pseudo-second order rate constant of adsorption of MB over RGO–CuS and bare CuS.

The removal efficiency was found to be 85 % for the RGO–CuS nanocomposite and 73 % for bare CuS. This shows a significant improvement in the adsorption capability of CuS after incorporation with RGO. The initial removal rate was faster than that at longer times, and usually after 60 min, the process became slower.

The kinetics of MB adsorption on RGO–CuS and CuS were also studied. The linear form of the pseudo-second-order rate equation was used. A pseudo-second-order kinetic fitting of (t/q_t) *vs*. t is shown in Fig. 6b. The correlation coefficients were found to be higher than 0.99, and the calculated equilibrium adsorption capacities (q_e values) were close to the experimental values for both RGO–CuS and bare CuS. Thus, the adsorption kinetics of MB could be satisfactorily described by a pseudo-second-order kinetic model. Fig. 6c shows the pseudo-second-order kinetic fitting for MB adsorption on RGO–CuS and CuS.

The rates of adsorption by these two materials are shown in Fig. 6d. The rate of adsorption of MB on RGO–CuS was much higher than that on CuS.

The data were fitted with the Langmuir (Fig. 7a) and Freundlich (Fig. 7b) models to compare the adsorption capacities of the synthesized materials. For this experiment, different concentrations of MB solutions (10, 20, 50, 70 and 100 ppm) were used with same amount of RGO–CuS adsorbent (1 mg mL^{-1}). The mixtures were stirred for 120 min at room temperature (25 °C).
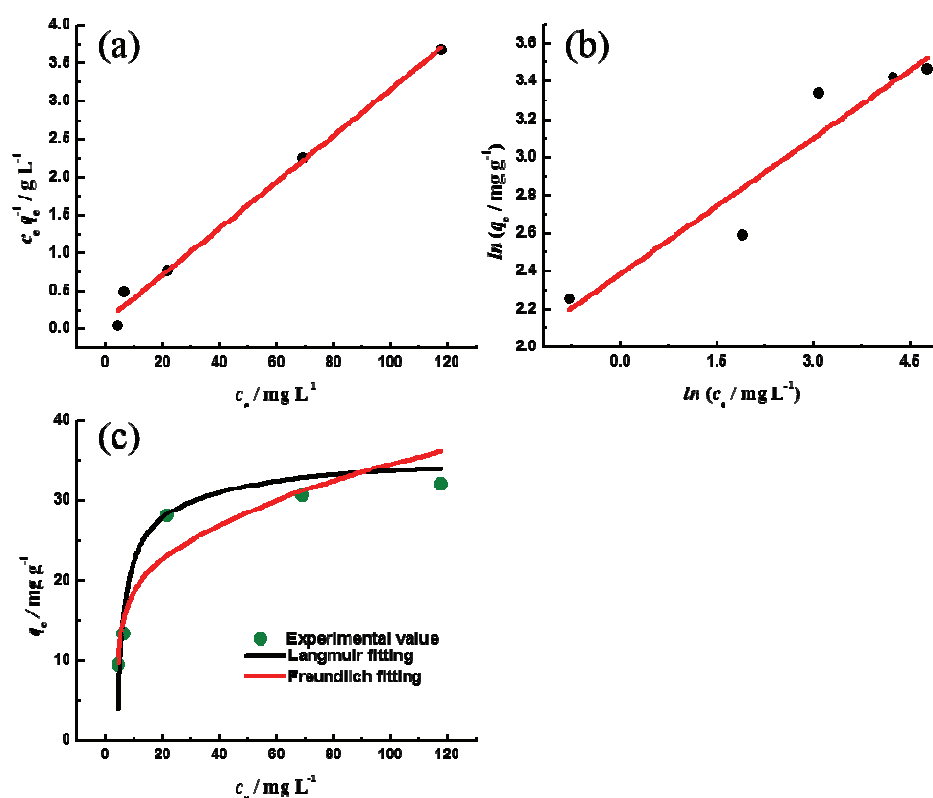

Fig. 7. a) Langmuir and b) Freundlich isotherms; c) Langmuir and Freundlich fitting isotherms for the adsorption of MB by RGO–CuS and CuS.

The Langmuir and Freundlich fitting isotherms of MB on RGO–CuS are shown in Fig. 7c. The fitting parameters and a comparison of the fitting data for the adsorption of MB on RGO–CuS derived in the present work are summarized in Table I. From Fig. 7 and Table I, it could be seen that the data are better fitted by the Langmuir model ($R^2 = 0.9887$), whereas a poorer fit was obtained by the Freundlich model ($R^2 = 0.8747$). As the data follow the Langmuir model, a monolayer adsorption process is suggested.

TABLE I. Parameters and a comparison of the fitting data for the adsorption isotherms

Parameter	Langmuir	Freundlich
q_m	32.78 mg g^{-1}	–
b	0.284 L mg^{-1}	–
K_f	–	10.89 mg$^{1-1/n}$ L$^{1/n}$ g^{-1}
n	–	4.2
R^2	0.98875	0.87467

The pH had a large effect on the adsorption of MB on the RGO–CuS nano-composite. The pH of the adsorption process was varied by adding HCl or NaOH. A 20 ppm MB solution was stirred with 1 mg mL^{-1} RGO–CuS adsorbent for 2 h at room temperature in the dark. Fig. 8 shows that at both acidic and basic pH, the adsorption is higher than that at neutral pH. The ionization of RGO–CuS is possible at high concentrations of ions (H^+ and OH^-), which opens up more sites for adsorption. As a result, the process becomes more favorable in media of high ionic concentration.
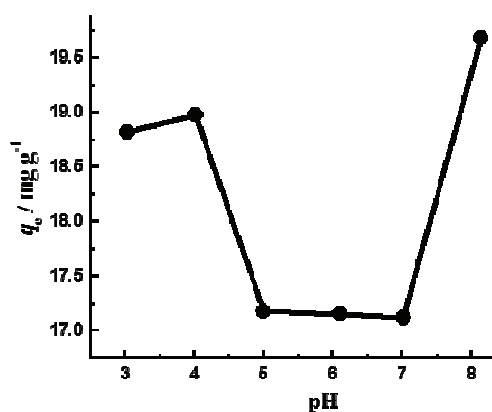

Fig. 8. Effect of pH on the adsorption of MB over RGO–CuS (room temperature).

Experiments were performed to determine the variation of the adsorption properties with temperature. At pH 6.1, the first stage of the adsorption was accelerated with increasing temperature but then decreased, as could be seen in Fig. 9. This temperature profile also helps in the calculation of the thermodynamic parameters for the MB adsorption process on RGO–CuS.

The thermodynamic parameters, such as Gibbs energy change (ΔG), enthalpy change (ΔH) and entropy change (ΔS) could be calculated.[26]

The calculated value of ΔG, ΔH and ΔS for the adsorption of MB on RGO–CuS are –4.23 kJ mol^{-1}, –1.5 kJ mol^{-1} and 5.11 J mol^{-1} K^{-1}, respectively. These values indicate that the process is an exothermic reaction (negative ΔH value) that occurs spontaneously (negative ΔG value). The values of the free energy and enthalpy changes suggest that the adsorption process is physical adsorption, according to Lie *et al*.[27] For general physical adsorption, the free

energy change is –20 to 0 kJ mol^{-1} and the enthalpy change is between 2 and 21 kJ mol^{-1}.[28] The present calculated values are near to the reported values. In physical adsorption, the adsorbate and the adsorbent are bonded with van der Waals force of attraction.
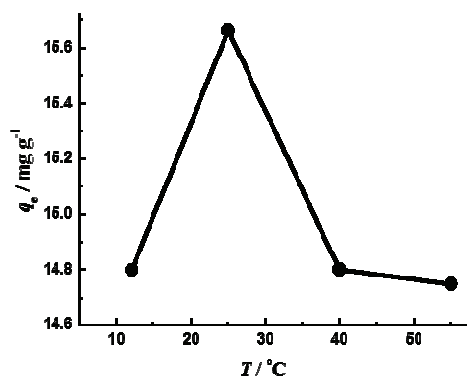

Fig. 9. Effect of temperature on the adsorption of MB over RGO–CuS (pH 6).

CONCLUSIONS

RGO was decorated with CuS nanoparticles using a hydrothermal reduction method. Characterization showed that the CuS nanoparticles were densely spread over the RGO sheets with a hexagonal crystal structure. The RGO–CuS nanocomposite exhibits significantly higher activity than bare CuS for the adsorption of MB in aqueous media. From the pH-dependent experiments, it was found that ionized media are more favorable for the adsorption of MB on RGO–CuS. It was estimated that the monolayer adsorption of MB on RGO–CuS follows pseudo-second-order reaction kinetics. From the thermodynamic parameters, it could be stated that the adsorption process is physisorption that is spontaneous and exothermic in nature.

ИЗВОД
ДОБИЈАЊЕ РЕДУКОВАНОГ ГРАФЕН-ОКСИДА СА НАНЕСЕНИМ НАНОЧЕСТИЦАМА CuS И ЊЕГОВА АКТИВНОСТ ПРЕМА АДСОРПЦИЈИ МЕТИЛЕНСКОГ ПЛАВОГ

FATIMA TUZ JOHRA и WOO-GWANG JUNG

School of Materials Science and Engineering, Kookmin University 77 Jeongneung-ro, Seongbuk-gu, Seoul 02707, Republic of Korea

Редуковани графен-оксид (RGO) може да служи као адсорбент због своје велике специфичне површине. Адсорпционе карактеристике су проучене на RGO композиту, комбинованом са CuS. Нађено је да ефикасност уклањања метиленског плавог износи 85 %, што је више него само са CuS (≈73 %). Осим тога, испитана је кинетика адсорпције метиленског плавог да би се одредио ред реакције. Процес уклањања је бржи са систе-

мом RGO–CuS него са само са CuS. Ни висока ни ниска температура није погодна за овај адсорпциони процес. У високо јонским срединама, високог или ниског pH, адсорпција је већа него при неутралним pH. Израчунати су термодинамички параметри, који указују да је реч о физисорпцији, егзотермне природе.

REFERENCES

1. S. Stankovich, D. A. Dikin, G. H. B. Dommett, K. M. Kohlhaas, E. J. Zimney, E. A. Stach, R. D. Piner, S. T. Nguyen, R. S. Ruoff, *Nature* **442** (2006) 282
2. F. Schedin, A. K. Geim, S. V. Morozov, E. W. Hill, P. Blake, M. I. Katsnelson, K. S. Novoselov, *Nat. Mater.* **6** (2007) 652
3. Z. He, Y. Zhu, Z. Xing, Z. Wang, *J. Electronic Mater*. **45** (2016) 285
4. X.-H. Guan, L. Yang, X. Guan, G.-S. Wang, *RSC Adv*. **5** (2015) 36185
5. M. N. Habashi, S. K. Asl, *Korean J. Mater. Res*. **27** (2017) 248
6. Q. Zhuo, Y. Ma, J. Gao, P. Zhang, Y. Xia, Y. Tian, X. Sun, J. Zhong, X. Sun, *Inorg. Chem.* **52** (2013) 3141
7. Y. He, Y. Liu, T. Wu, J. Ma, X. Wang, Q. Gong, W. Kong, F. Xing, Y. Liu, J. Gao, *J. Hazard. Mater*. **260** (2013) 796
8. H. R. Pouretedal, A. Norozi, M. H. Keshavarz, A. Semnani, *J. Hazard. Mater*. **162** (2009) 674
9. M. Ghaedi, M. Pakniat, Z. Mahmoudi, S. Hajati, R. Sahraei, A. Daneshfar, *Spectrochim. Acta, Mol. Biomol. Spectrosc*. **123** (2014) 402
10. Y. Zhang, J. Tian, H. Li, L. Wang, X. Qin, A. M. Asiri, A. O. Al-Youbi, X. Sun, *Langmuir* **28** (2012) 12893
11. W. Sun, J. Zhong, B. Zhang, K. Jiao, *Anal. Bioanal. Chem*. **389** (2007) 2179
12. J. Qian, K. Wang, Q. Guan, H. Li, H. Xu, Q. Liu, W. Lie, B. Qie, *Appl. Surface Sci*. **288** (2014) 633
13. C. Hu, Y. Liu, J. Rong, Q. Liu, *Nano: Brief Rep. Rev.* **8** (2015) 1550123
14. J. Shi, X. Zhou, Y. Liu, Q. Su, J. Zhang, G. Du, *Mater. Lett*. **126** (2014) 220
15. Y. Wang, L. Zhang, H. Jiu, N. Li, Y. Sun, *Appl. Surface Sci*. **303** (2014) 54
16. K.-J. Huang, J.-Z. Jhang, Y. Liu, Y.-M. Liu, *Int. J. Hydrogen Energy* **40** (2015) 10158
17. W. Choi, I. Lahiri, R. Seelaboyina, Y. S. Kang, *Crit. Rev. Solid State Mater. Sci*. **35** (2010) 52
18. H. Feng, R. Cheng, X. Zhao, X. Duan, J. Li, *Nat. Commun*. **4** (2013) 1539
19. F. T. Johra, W.-G. Jung, *Appl. Surface Sci*. **362** (2016) 169
20. S. Sun, D. Deng, C. Kong, X. Song, Z. Yang, *Dalton Trans*. **41** (2012) 3214
21. G. D. Smith, R. J. H. Clark, *J. Cult. Herit.* **3** (2002) 101
22. T. P. Mernagh, A. G. Trudu, *Chem. Geol*. **103** (1993) 113
23. A. C. Ferrari, J. Robertson, *Phys. Rev., B* **61** (2000) 14095
24. F. Tuinstra, J. L. Koenig, *J. Chem. Phys*. **53** (1970) 1126
25. S. Park, J. An, I. Jung, R. D. Piner, S. J. An, X. Li, A. Velamakanni, R. S. Ruoff, *Nano Lett*. **9** (2009) 1593
26. B. I. Olu-Owolabi, P. N. Diagboya, W. C. Ebaddan, *Chem. Eng. J.* **195** (2012) 270
27. Z. Liu, F.-S. Zhang, *J. Hazard. Mater.* 167 (2009) 933
28. P. W. Atkins, *Physical Chemistry*, 4th ed., Oxford University Press, London, 1990, p. 884.